Diode Laser

Matthias Pospiech, Sha Liu

20th December 2003

Contents

1 theory

1.1 diodelaser

laser in general

to achieve laser action, a device must contain a gain element located in an optical resonator. The gain element is composed of a material that is able to support a population inversion when excited, a photon passing through a gain element has a higher probability of producing a second photon at the same wavelength by stimulated emission. A resonator is required for the generation of optical feedback [Sch02].

Semiconductor lasers operate by passing current through a p-n junction. Electrons travelling in the n region have more energy than those in the p region, when the electron passes from n to p, the excess energy is lost by photon emission. Here the resonator mirrors are the end faces of the semiconductor chip itself. [GPA93]

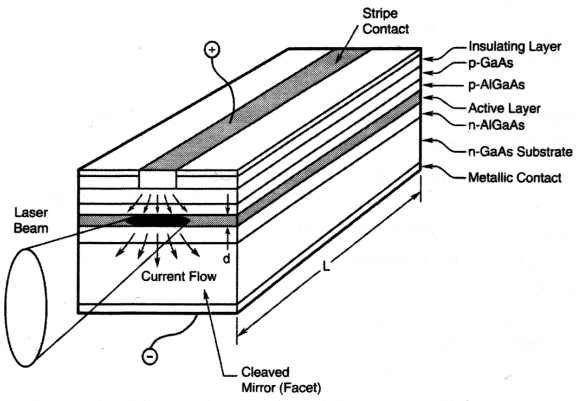

Figure 1: principal setup of a diode laser

Figure 1 gives the schematic illustration of the double-heterostructure semiconductor laser model with typical physical dimensions. The dotted area represents the depletion region in the vicinity of the homojunction. The hatched area shows the thin (0.2μ) active layer of a semiconductor material whose band gap is slightly lower than that of the surrounding cladding layer.

In the heterostructure device, the threshold current reduces. There are two reasons: first, the cladding layers surrounding the active layer have a higher band gap. The band-gap difference confines the electrons and holes to the active layer, where they recombine to produce the optical gain. Second, it has a comparatively lower refractive index than the active layer. The refractive-index difference confines the optical mode close to the active layer, which significantly reduces the internal loss. As one can see from figure 2. [GPA93].

Laser threshold

When the current is applied to the semiconductor laser, the laser does not emit coherent light until the current exceeds a critical value, known as the threshold current. This is

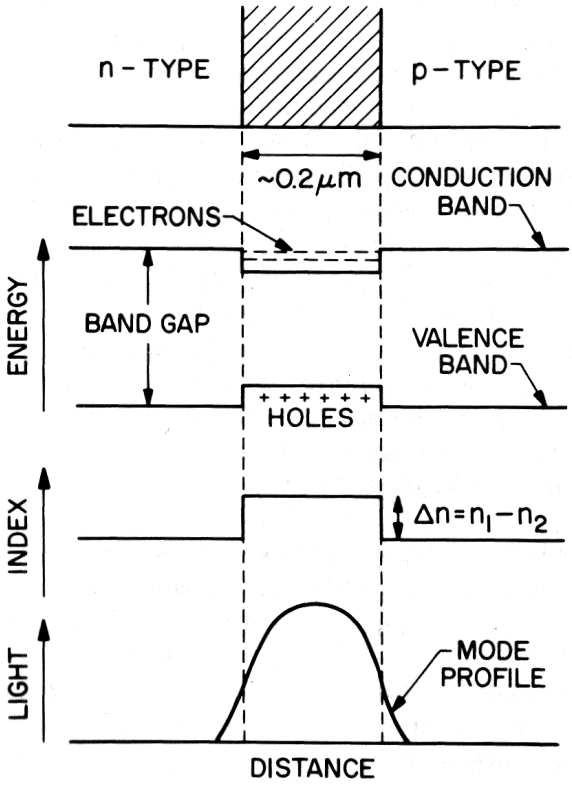

Figure 2: structure of a diode laser

because stimulated emission has to compete against the absorption process during which an electron-hole pair is generated at the expense of an absorbed photon. Since the electron population in the valence band generally far exceeds that of the conduction band, absorption dominates. At a certain value of the external current, a sufficient number of electrons are present in the conduction band to make the semiconductor optically transparent. With a further increase in current, the active region of the semiconductor laser exhibits optical gain and can amplify the electromagnetic radiation passing through it.

The other necessary ingredient is optical feedback. In semiconductor laser it is provided by the cleaved facets that form an FP cavity. The role of the FP cavity is towfold. First, it provides a direction selectivity for the process of stimulated emission, since only photons along its axis are reflected back and forth. Second, it provides a wavelength selectivity since the feedback is strongest for wavelengths corresponding to the longitudinal modes of the FP cavity.

In the above-threshold regime, laser output increases almost linearly with the current. Almost all electrons and holes injected into the active region now recombine through stimulated emission, and the internal quantum efficiency approaches 100%. Over a narrow current range in the vicinity of the threshold current, the output power jumps by several orders of magnitude and the spectral width of the emitted radiation narrows considerably because of the coherent nature of stimulated emission [GPA93].

Temperature tuning

The center wavelength of a laser diode shifts with junction temperature by 0.3nm/°C. Diode life time decrease dramatically as the operating temperature increases. There are some practical issues to note regarding diode cooling. First, the thermal conductivity of the semiconductor substrate is quite low, so a significant amount of cooling is required to keep the junction's working temperature. Second, care must be taken to consider the dew point of the operating environment. Water condensation on the diode or on the optical window of a hermetically sealed housing will degrade the laser diode output. An additional caution is that cooling should be applied only when running the diode, as the diode may otherwise get too cold when the drive current is not heating the junction [Sch02].

Current tuning and mode hop

As the diode power is increased by applying more current to the junction, the temperature increases, thereby red-shift the diode output wavelength. A second effect related to the drive current is tuning due to the changing density of electrons in the junction. The electron density affects the refractive index of the active layer and determines the frequency of the FP resonator modes. The wavelength shift due to current density changes is about 0.03nm/A.

Mode hopping is a phenomenon that prevents continuous tuning of a laser diode output wavelength over a range that is wide compared to the intermodal spacing. Adjacent diode resonator modes are separated by a certain nm, these modes are superimposed on the broad spectral gain profile of the active layer. As the temperature changes, the peak of the gain spectrum shifts. At some point, the gain for the wavelength represented by an adjacent longitudinal mode will be higher than the gain at the longitudinal that has been oscillating. At this point, the diode demonstrates an instability or "'mode hop"' The output wavelength shifts discontinuously from the n to $n \pm 1$ mode [Sch02].

Temperature-frequency, current-frequency dependence

$$\lambda(T, I) = \lambda(T_0, I_0) + \alpha_T(T - T_0) + \alpha_I(I - I_0) + \sum_{k=2}^{n} \left\{ \alpha_T^k (T - T_0)^k + \alpha_I^k (I - I_0)^k \right\} \quad (1)$$

Usually, the wavelength obeys(0,05nm/K) (from paper 'Versuch 2,11')
Here we expand the wavelength into a polynomial, with the 0th order is a constant, the 1st order is linear with temperature and current, and the high order is comparatively small, and can be neglected.

1.2 cavities (Fabry Perot)

principle of optical cavities

In its basic assembly optical cavities consist of two facing highreflective mirrors (distance L) with specific radii of curvature (R) and different transmission T. Typical reflectivities are 99.9% for the incoupling mirror and 98.0% for the outcoupling mirror. Thus the laserbeam between the mirrors is reflected back and forth which forms a standing wave. This assembly

is labeled 'Fabry Perot Cavity' in contrast to 'ring resonators' where we have a traveling wave in just one direction. [Sie86]

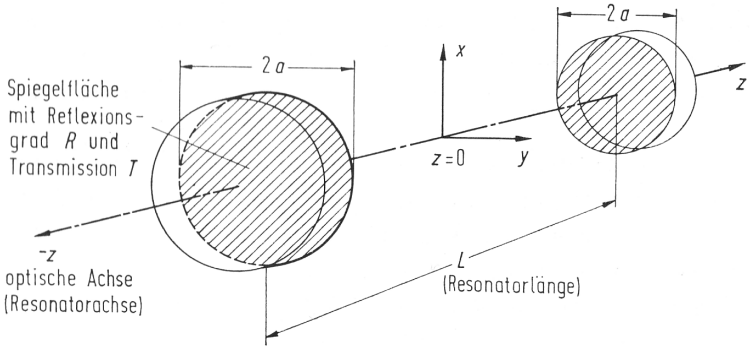

Figure 3: assembly of a Fabry-Perot cavity

The important properties of such an optical cavity is caused by interferences of the back and forth reflected beam inside the mirrors. Not only does this increase the energy inside the cavity by a huge amount, but makes the cavity as well only resonant for specific frequencies. Additionally takes the intensity distribution of the laserbeam inside the cavity (transverse modes) a different shape depending on the type of cavity and its length. An optical cavity is thus characterized by its resonant frequencies, transverse modes, and its ability to store electromagnetic energy.

Cavities with flat mirrors are unfortunately very unstable for long distances L between the mirrors. If these are not perfectly parallel the beam will easily walk out of the mirrors. One uses therefore cavities with different mirrors and distances that overcome the problem of beam-stability.

types of cavities

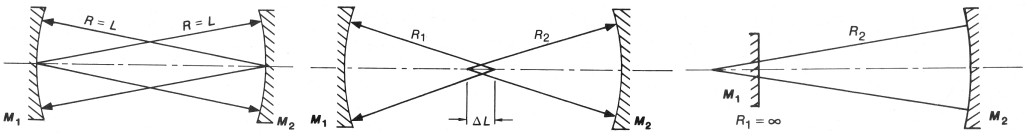

(a) confocal (b) concentric (c) hemispherical

Figure 4: types of optical cavities

The mirrors have these proportions with the length of the cavity: [Sie86]

- confocal (symmetric): $R_1 = R_2 = L$
- concentric (symmetric): $R_1 = R_2 = 1/2L$
- hemispherical: $R_1 = \infty, R_2 = R, L < R$

The type of cavity used in this experiment is of the confocal type.

resonator modes

In analogy to mechanics describe modes in laseroptics vibrational-modes of the electromagnetic wave in the cavity. Transversal modes differ thereby in their distribution of intensity perpendicular to the axis of the resonator, the longitudinal modes contrary in direction of the axis.

transversal modes

Stationary solutions of the superposition of the back and forth reflected waves are called 'stationary field distributions'. This means that the amplitude distribution of the electromagnetic field stays unchanged with time. Each transversal mode corresponds to a different stationary field distributions.

Linear waves (straight wavefronts) can not form stationary field distributions due to diffration effects. Owing to their diffration losses at the border of the mirrors which are greater than those in the middle the field distribution would change with each reflection, so that stationary distributions will not be achieved with this kind of field distribution.

The stationary distributions can be calculated with the 'Fresnel Integral' [Dem00]. Analytic solutions are only possible for the confocal resonator. These solutions are the Hermite-Gauss oder Laguerre-Gauss modes.

Depending on the symmetry of the cavity one uses cylinder-coordinates (for circular mirrors) or cartesian-coordinates (for rectangular mirrors). In the former case one obtains the Laguerre-Gauss modes TEM_{pq}, and for the latter the Hermite-Gauss modes TEM_{mn}. [ILT]

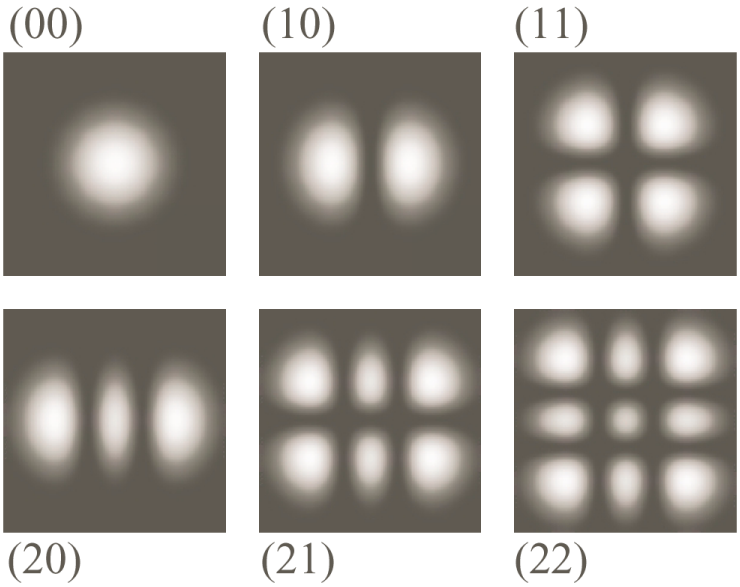

Figure 5: Hermite-Gauss modes TEM_{mn} [Mes99]

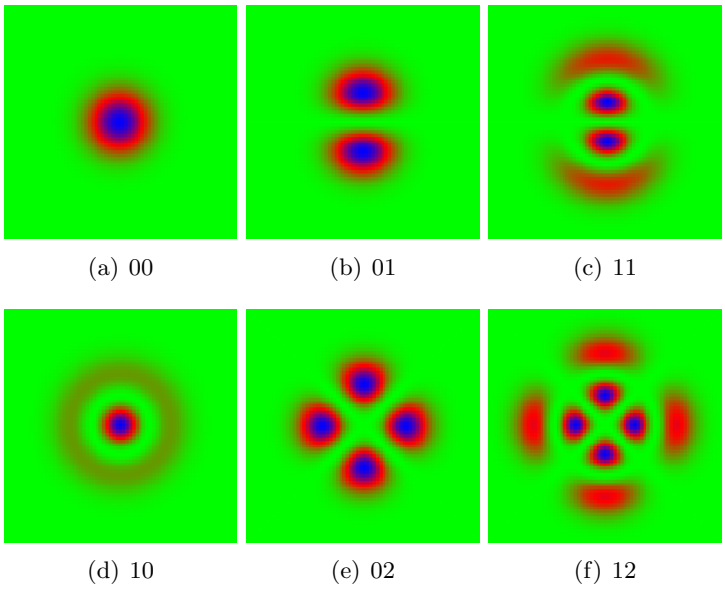

(a) 00 (b) 01 (c) 11

(d) 10 (e) 02 (f) 12

Figure 6: Laguerre-Gauss modes TEM_{pq} [ILT]

gauss-mode

The basic mode TEM_{00} is called the Gauss-mode. This name has its origin in the amplitude distribution. The Gaussian-beam has a gauss-profile in the radial intensity.

longitudinal modes

We have in addition to the transverse modes longitudinal modes in the cavity. These are standing waves in the resonator. The resonant frequencies ν_{mnq} of longitudinal modes depend on the transverse mode and the length of the cavity. Modes are therefor full described by the indices m, n (transversal) and q (longitudinal): TEM_{mnq}.

The condition for longitudinal modes in the simple case of two flat mirrors is, that the length L of the cavity is a full multiple number of the half of the wavelength q:

$$L = \frac{\lambda}{2} q \qquad \Rightarrow \nu = \frac{c}{2L} q$$

whereas for different mirrors the condition for resonant frequencies changes to:

$$\nu_{mnq} = \frac{c}{2L} \left[q + (m + n + 1) \cdot F \right] \qquad q : \text{full number} \tag{2}$$

with factor F for different cavity types. In case of the confocal resonator this is $1/2$ for F [Sie86].

free spectral range (FSR)

The free spectral range $\delta\nu$ denotes the frequency spacing between two modes. For transversal modes this is: $(\Delta(m+n)=1)$

$$\delta\nu = \frac{c}{4L}$$

and for longitudinal modes: $(\Delta q = 1)$

$$\delta\nu = \frac{c}{2L}$$

This is often denoted as Δ_{FSR}.

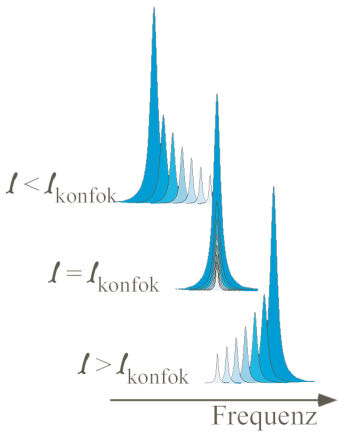

Figure 7: spectrum of almost confocal cavities

mode selection

In general several modes oscillate in the cavity. Due to different losses for different modes in the cavity will the basic modes be preferred. In case that the cavity is not adjusted to the confocal case $(R = L)$ do higher modes oscillate as well. In the frequency spectrum are then more modes with different resonant frequencies visible, so that the free spectral range can not be observed. This behavior is displayed in figure 7.

spectral resolving power of the Fabry-Perot cavity

The resolution of the transmission line of the cavity is depending on the losses inside the cavity very high - but this is of less interest because only frequency differences can be measured. The 'resolution' that plays a role in our measurements is instead proportional on the free spectral range Δ_{FSR}.

1.3 grating monochromator

Gratings are a common tool for frequency resolution measurements. They have a frequency or angle dependend diffraction of light due to interference effects. Of interest is only the first order of diffraction. In practice are mainly reflection gratings used The diffraction for incidented waves is described by the grating-equation:

$$m\lambda = d(\sin\alpha + \sin\beta) \tag{3}$$

(m:order of diffraction, d: separation of lines, α: incoming angle, β: diffraction angle)

Hence frequency resolution measurements are possible if one fixes the incoming angle and measures the angle β (or vice versa) with changing wavelength λ.

The spectral resolving power of the grating is determined by the formula

$$\frac{\lambda}{\Delta\lambda} \leq mN \tag{4}$$

and thus depends on the order m used and the Number N of illuminated grating-lines. The term $\Delta\lambda$ is the lowest wavelengthdifference at which lines can be separated. The wavelength λ is thereby defined as $\lambda \equiv \sqrt{\lambda_1\lambda_2}$.

The grating monochromator used in this experiment uses a fiber for the light input, which is then incidented on the grating. The intensity of the selected wavelength is measured by a photodiode which supplies a voltage on the output of the monochromator. The wavelength can then be scanned by rotation of the grating with the attached equipment.

1.4 Structure of Rb - the D2 transition

The structural underpinnings of Rb responsible for the transition of an electron from one state to another is as follows: the ground state electron configuration of Rb is [1s2, 2s2, 2p6, 3s2, 3p6, 3d10, 4s2, 4p6, 5s1]. Only the valence shell (5s) is unfilled with one electron. As a result, the structure of energy levels is similar to that of hydrogen. As for the core Rb+ ion, it is spherically symmetric, resulting in a total angular momentum (L), spin angular momentum (S), and thus spin-orbit $L-S$ coupled angular momentum ($J = |J| = |L+S|$) of zero. Consequently, with all the core ion quantum numbers equal to zero, the observed energy transitions with the associated changes in $L-S$ coupled quantum numbers comes from the valence electron only. Stated in L-S coupling notation: $(\mathrm{nl})^{2S+1}L_j$, (where n and l are the principle and angular momentum quantum numbers respectively), the ground electronic state is (5s) $^2S_{\frac{1}{2}}$, and the first electronic excited state is found in the $(5\mathrm{p})^2P_{\frac{3}{2},\frac{1}{2}}$ orbital. Here $S = 1/2$ and $L = p = l$, leaving two possible values for J (i.e., $|L-S|$, ?, J, ?, |L+S|; in integer steps) equal to 1/2 and 3/2 . As a result, two possible energy levels exist for these given n and l values. The first, less energetic excited state is referred to as the D1 line and has the following quantum numbers: $(5\mathrm{p})^2P_{\frac{1}{2}}$. The second, more energetic excited state is referred to as the D2 line and has these quantum numbers: $(5\mathrm{p})^2P_{\frac{3}{2}}$.

This splitting of the $S = 1/2$ and $L = 1$ state into two finer ($J = 1/2$, and $3/2$) states is known as the magnetic fine structure states of the atom, where the former state corresponds to a transition from the ground state with a wavelength of 794.8 nm, whereas the latter transition corresponds to a wavelength of 780.0 nm. Our diodelaser can only be tuned in and around 780.0 nm, and therefore we concentrate on the D2 line.

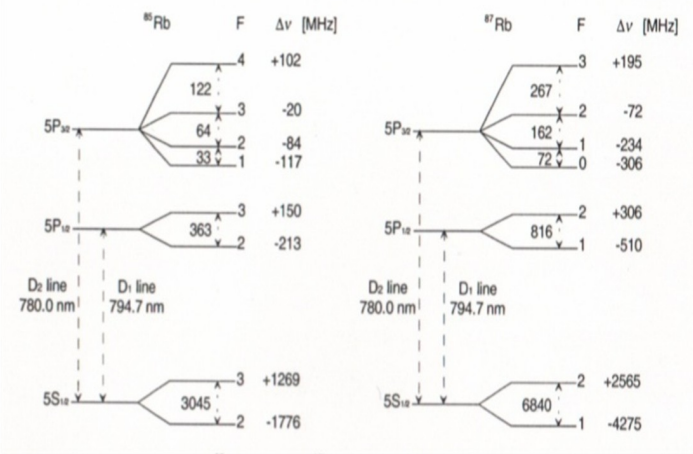

Figure 8: energy manifold of the Rb D_2 transmission

2 measurements

2.1 current - voltage dependence

We set the temperature at 17°C and increase the current from 30mA by steps of 5mA. In the interval of 40mA and 45mA the current increases dramatically, so that we set the step value down to 1 mA to get more data in the threshold region. After the threshold we measure the current up to 115mA in the steps of 5mA again.

The laserbeam is adjusted on the photodiode, so that we can get a dependence of current vs. voltage.

setup

In the distance of about 20cm away from the diode the waist of the beam was due to the divergence a few millimeter wide. The first idea was then to compensate the divergence of the beam. With the lenses available it was unfortunately not possible to realize a straight beam profile. We then have inserted a 200 mm lens directly after the laserdiode which has its focus in the region of our detectors (photodiode, fiber).

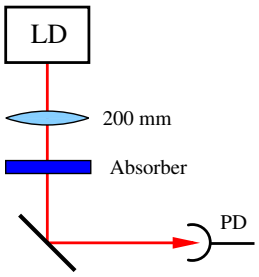

The absorber was necessary to ensure that we do not exceed the working range of the photdiode. This absorber has an increasing absorption over its length. Once set to a position this was not changed anymore thoughout the experiment.

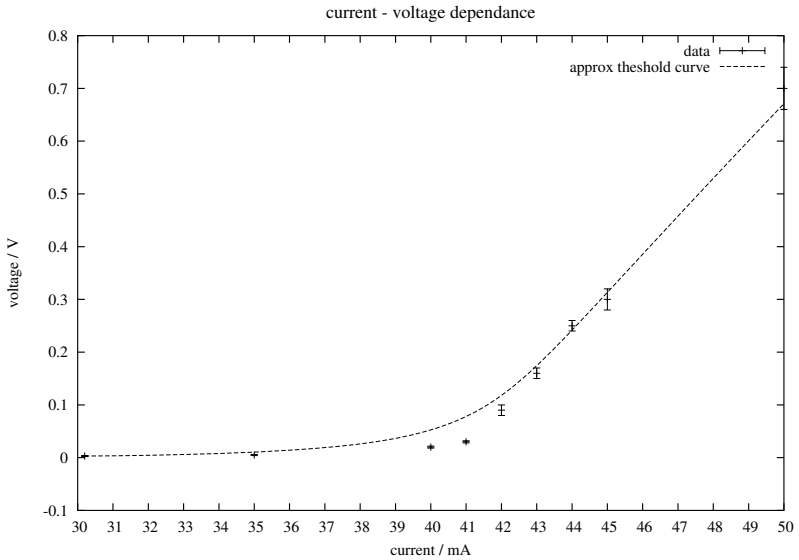

Figure 9: current vs. voltage in the threshold regime

From this data we can conclude that the threshold of the laserdiode at 17°C is approximately at 41 mA.

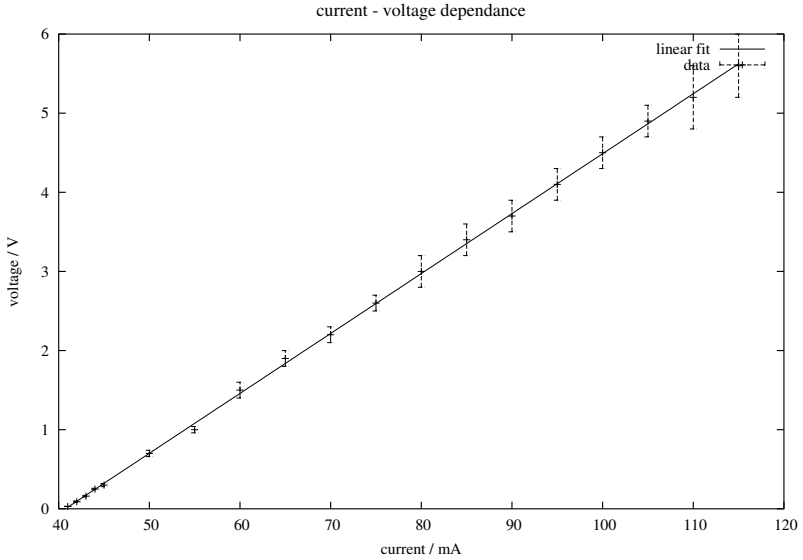

Figure 10: current vs. voltage with the diode in the laser regime

This measurement shows the linear dependence between current and voltage (power) as expected.

I /mA	position	scale	U / V	ΔI / mA	ΔU / V
30.2	0.6	0.005	0.003	0.05	0.001
35.0	1.0	0.005	0.005	0.05	0.001
40.0	1.6	0.01	0.02	0.05	0.002
41.0	3.0	0.01	0.03	0.05	0.002
42.0	1.7	0.05	0.09	0.05	0.01
43.0	3.2	0.05	0.16	0.05	0.01
44.0	4.9	0.05	0.25	0.05	0.01
45.0	0.3	0.1	0.3	0.05	0.02
50.0	3.5	0.2	0.7	0.05	0.04
55.0	5.2	0.2	1.0	0.05	0.04
60.0	2.9	0.5	1.5	0.05	0.1
65.0	3.7	0.5	1.9	0.05	0.1
70.0	4.4	0.5	2.2	0.05	0.1
75.0	5.2	0.5	2.6	0.05	0.1
80.0	3.0	1.0	3.0	0.05	0.2
85.0	3.4	1.0	3.4	0.05	0.2
90.0	3.7	1.0	3.7	0.05	0.2
95.0	4.1	1.0	4.5	0.05	0.2
105.0	4.9	1.0	4.9	0.05	0.2
110.0	2.6	2.0	5.2	0.05	0.4
115.0	2.8	2.0	5.6	0.05	0.4

Table 1: Current - Voltage

2.2 current - power dependence

The process of measurement is mainly the same as before. The main difference is the use of a powermeter (portable device by Coherent). This has been fixed to get suitable results - it is meant to be used by holding it with hand inside the beam, but that can only give the approximate magnitude of the laserbeam's power. After we had fixed it we could much better reproduce a measurement by doing a series of measurements at the same value of current. The error of the powermeter was assumed to be 10 percent.

The number of steps has been decreased here since the accuracy of the device is lower than the photodiode, so that we did not want to reproduce the curve of threshold and linear increase here. Nevertheless we can see a linear dependence between current and power. (The threshold region is omitted in this graph)

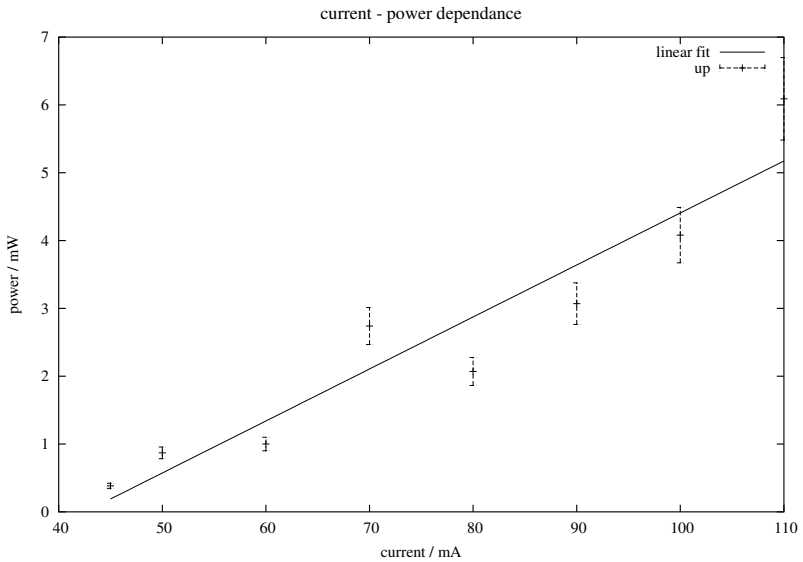

Figure 11: current-power

I / mA	Power / mW	ΔI / mA	Power / mW
110.0	6.09	0.05	0.61
100.0	4.08	0.05	0.41
90.0	3.07	0.05	0.31
80.0	2.07	0.05	0.21
70.0	2.74	0.05	0.27
60.0	1.00	0.05	0.10
50.0	0.87	0.05	0.09
45.0	0.38400	0.05	0.04
40.0	0.02210	0.05	0.00
35.0	0.00882	0.05	0.00
30.0	0.00576	0.05	0.00

Table 2: Current - Power

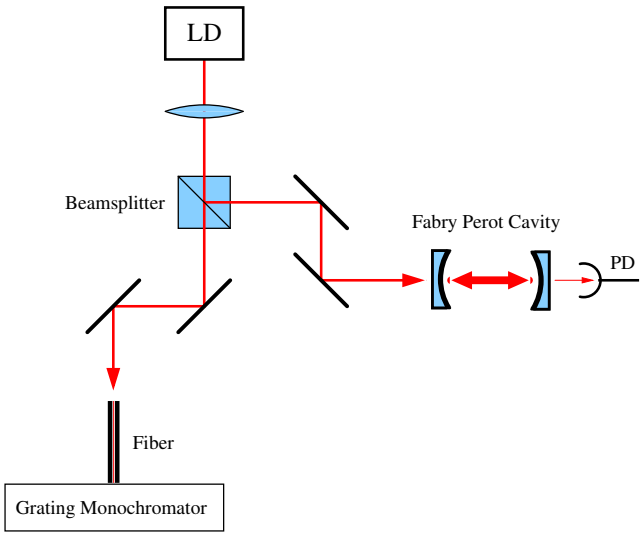

new setup of optical desk

For the following experiments we have reorganized the optical desk to be able to do all the experiments without any change or additional adjustments. We used for the fiber as well as for the cavity two mirrors to adjust the beam. This is necessary to adjust position and angle of the beam independently (beam-walk). The adjustment for each measurement unit is discussed with the measurement.

2.3 resolution of grating monochromator

The laser beam was focused into the fiber with the CCD Camera and the IR-Fluorescence Card. The output of the monochromator was first attached to the oscilloscope to find the maximum of the laser. From this we have decided to scan from 780 - 782 nm. For the actual measurement we kept current and temperature fixed. The output is now attached to the x-y-writer. For the calculation of the halfwidth we have taken notes of the starting and end wavelength on the monochromator and have started and stopped the x-y-writer with the monochromator co-instantaneously. Thus the length on the paper is directly related to the wavelengthdifference on the monochromator. The slid-width was changed from 600μm to 300μm in steps of 50μm. The corresponding paper can be found in the appendix. From the paper we measure the full width at half maximum (FWHM).

slitwidth / μm	λ_S /nm	λ_E /nm	$\lambda_E - \lambda_S$/nm	Δx /cm	nm per cm
600	779.9	782.7	2.8	11.05	0.25
550	780.6	782.7	2.1	7.35	0.29
500	780.3	782.6	2.3	8.05	0.29
450	780.3	782.5	2.2	7.55	0.29
400	780.2	782.4	2.2	8.35	0.26
350	779.9	782.3	2.4	8.45	0.28
300	780.0	782.4	2.4	8.50	0.28

Table 3: resolution of grating: data

Peak /cm	Peak /nm	FWHM /cm	FWHM /nm	$\lambda/\Delta\lambda$
7.8	781.88	2.75	0.70	1122.04
4.4	781.86	2.35	0.67	1164.47
5.8	781.96	2.05	0.59	1335.05
5.5	781.90	1.65	0.48	1626.27
6.5	781.91	1.25	0.33	2374.17
6.8	781.83	0.90	0.26	3058.55
6.6	781.86	0.55	0.16	5034.73

Table 4: resolution of grating: data

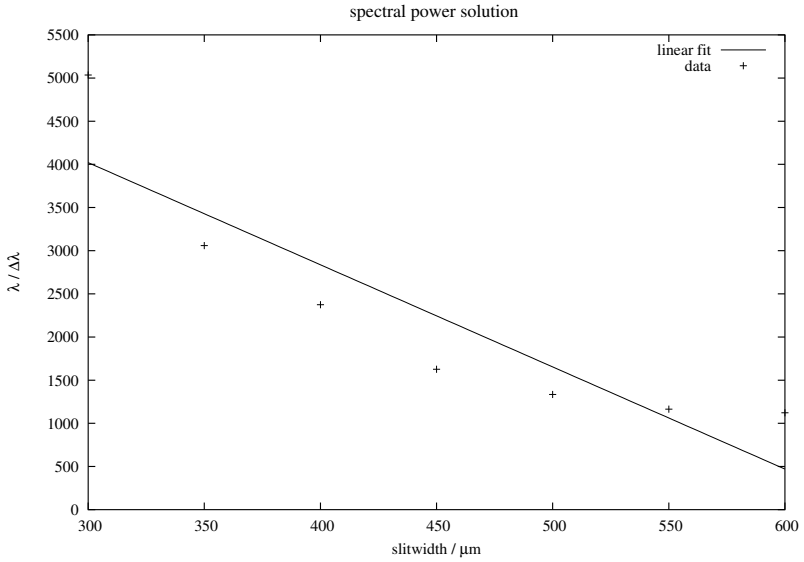

Figure 12: spectral resolving power vs. slitwidth

We do not only want a high resolution but we are also interested in the intensity of light incidented on the grating. The latter should be high enough to give suitable data. Since the intensity decreases with lower slitwidth we have chosen a slitwidth of 400 nm for the further experiments because it seemed to be a reasonable value.

2.4 resolution of the Fabry-Perot-cavity

adjustment of the Fabry-Perot-cavity

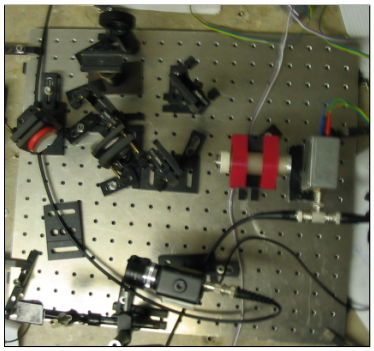

Before any adjustment on the cavity was done, we have taken care that the hight of the beam was as constant as possible and that the beam was always in the center of the mirrors. Then the beam was first roughly adjusted into the photodiode without the cavity and then the cavity inserted and moved into the best position.

We still do not know how well the beam passes through the cavity and cannot determine this from looking at the way of the laserbeam. To optimize this we put the CCD camera directly behind the cavity. What you see than are two bright centers. We tried to bring these two bright spots together and simultaneously tried to achieve an equally distributed brightness on the screen. This is then the gauss-ground mode, which appears as circles on the screen. With this we can be sure to have the light in the center axis of the cavity. The modes that can be seen during this process are shown in figure 13.

The resonant lines of the cavity are very likely not matched with the frequency of the laserdiode. Hence we use the frequency-generator (84 Hz) to tune the frequency of the laserdiode. This frequency-generator produces a zigzag curve (not sinus) with linear increase and decrease of voltage which is connected to the DC input of the current driver.

On the photodiode we now see a very hight number of resonant modes in the tuning range on the oscilloscope. This is due to the fact that the cavity is not yet adjusted to the confocal case, so that all the higher modes are not degenerated and appear all separate. To adjust to the confocal case we change the length of the of the cavity until all lines coincidence (a few peaks with equal distances). Finally we adjust the position of the photodiode again to be in the maximum. It appeared thereby that the intensity of the light incidented into the photodiode was out of its range. Therefore we had to install the absorber again, which we did as shown on page 11.

modes of the cavity

The adjustment of the Fabry Perot cavity was a good time to take a closer look at the different modes of the cavity as well. The dejustment of the beam inside the cavity with the mirrors lead to the preference of higher modes. Thus we only needed to dejust the beam to find higher modes. Some of the modes that could be observed are shown in figure 13. Of special interest are picture (a) with the ground mode TEM_{00} and picture (f) which shows a Laguerre-Gauss mode TEM_{03}. The latter is surprising because Laguerre-Gauss modes can only be resonant if the there is a perfect radial symmetry which is very easily broken.

Picture (b) and (c) show a typical picture of a dejusted beam with a nonradial brightness distribution. Picture (d) and (e) show modes of the order of 10, but we can not assign them to a mode.

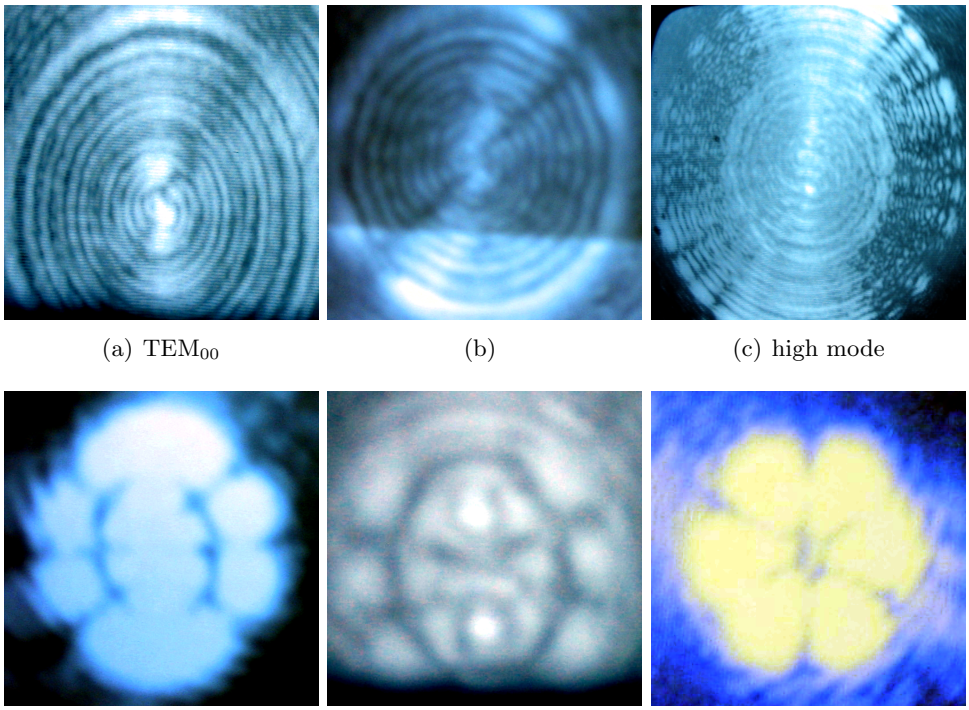

(a) TEM_{00} (b) (c) high mode

(d) (e) (f) TEM_{03}

Figure 13: different modes of the cavity

resolution measurement

With the frequency generator that comes with the experiment a measurement of the resonant lines of the cavity was not possible. The lines cannot be read from the oscilloscope and the 84 Hz of the generator were much too fast for the x-y-writer. We used therefor a different, more sophisticated wave-generator. This was then set to 40 mHz and an Amplitude of 2VPP, so that we could write the output of the photodiode on the x-y-writer (25 cm/min). The record of this is attached in the appendix.

Evaluations with this graph can unfortunately not be done since there is no known relationship between voltage amplitude for the DC-input of the current driver and the frequency generated. Nevertheless one can see that the linewidth is very low in the cavity.
Anyway is the effective resolution for our measurements not the linewidth of the resonances but rather the free spectral range. That is according to the theory in section 1.2 with $L = 5cm$:

$$\Delta_{\mathrm{FSR}}(\nu) = \frac{c}{4L} \approx 1.45\mathrm{GHz} \tag{5}$$

This value in wavelength difference calculated with $\lambda = 780\mathrm{nm}$ and

$$\Delta_{\mathrm{FSR}}(\lambda) = \lambda - (\lambda + \Delta\lambda) = \lambda - \frac{c}{\nu + \Delta\nu} = \lambda - \frac{c}{\frac{c}{\lambda} + \Delta\nu} \approx 2.9 \cdot 10^{-12}\mathrm{m} = 2.9\mathrm{pm} \tag{6}$$

2.5 temperature - frequency dependence

The setup shown on page 14 was used for this and the next experiment. We assume the errors as $\Delta\lambda = 0.04\text{nm}$, $\Delta T = 0.04°\text{K}$, $\Delta(\text{lines}) = 0.2 - 0.5$.

grating monochromator

We set the current at a fixed value (94.0 mA), and then increased the temperature from 10°C to 18.5°C in steps of 0.5°K. Using the grating monochromator we can see the peak of each frequency and keep record of the corresponding wavelength. Afterwards we change the current from 18.5°C down to 10°C in steps of 0.5°K and measure with the grating in the same way again. Usually it takes long time for the temperature to get stable in the rising period than in the decreasing period.

FP cavity

The laser frequency is scanned with the sinus generator connected to the DC input of the current driver. The current thereby is fixed at 71.9 mA. The output of the generator should be kept low, so the frequency will not be influenced much. The length of the Fabry-Perot-resonator was adjusted just equal to the radius of the reflected mirror (confocal case) as described.

So we can see the free spectral range (FSR) very clearly, as a series of simple peaks. We then measure in a circle to turn the temperature from 10.0°C to 18.5°C and back to 10.0°C in steps of 0.5°K. In each step we count how many lines pass by. Since the cooling is very fast, we need to turn the crew slowly to discrete the passing lines.

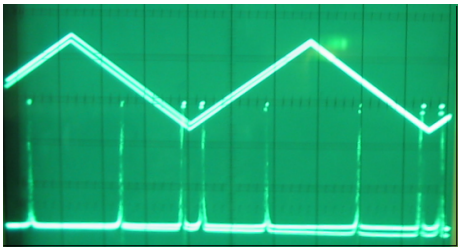

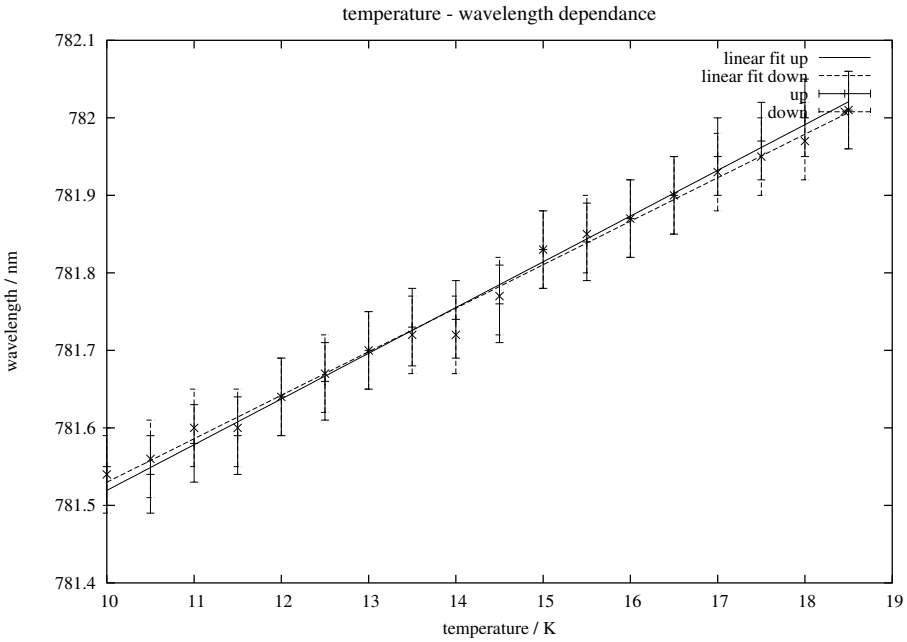

Figure 14: temperature-frequency (Monochromator)

Monochromator		
T/°C	λ/nm forward	λ/nm backward
10.0	781.55	781.54
10.5	781.54	781.56
11.0	781.58	781.60
11.5	781.59	781.60
12.0	781.64	781.64
12.5	781.66	781.67
13.0	781.70	781.70
13.5	781.73	781.72
14.0	781.74	781.72
14.5	781.76	781.77
15.0	781.83	781.83
15.5	781.84	781.85
16.0	781.87	781.87
16.5	781.90	781.90
17.0	781.95	781.93
17.5	781.97	781.95
18.0	782.00	781.97
18.5	782.01	782.01

Table 5: Temperature - wavelength

Fabry-Perot-resonance						
T_{end}	$\Delta lines_{\downarrow}$	$\Delta lines_{\uparrow}$	$\Delta\nu_{\downarrow}$	$\Delta\nu_{\uparrow}$	$\sum\nu_{\downarrow}$	$\sum\nu_{\uparrow}$
10.5	5.5	7.5	7.98	11.60	7.98	11.60
11.0	6.0	8.5	8.70	10.88	16.68	22.48
11.5	6.0	7.5	8.70	12.33	25.38	34.80
12.0	6.0	8.5	8.70	10.88	34.08	45.68
12.5	6.0	8.5	8.70	12.33	42.78	58.00
13.0	6.0	8.5	8.70	12.33	51.48	70.33
13.5	6.0	8.0	8.70	12.33	60.18	82.65
14.0	6.0	8.0	8.70	11.60	68.88	94.25
14.5	5.8	8.0	8.41	11.60	77.29	105.85
15.0	6.2	7.5	8.99	11.60	86.28	117.45
15.5	6.2	8.0	8.99	10.88	95.27	128.33
16.0	6.0	7.5	8.70	11.60	103.97	139.93
16.5	6.2	8.0	8.99	10.88	112.96	150.80
17.0	6.5	6.5	9.43	11.60	122.38	162.40
17.5	6.2	7.5	8.99	9.43	131.37	171.83
18.0	7.0	7.0	10.15	10.88	141.52	182.70
18.5	8.2		11.89	10.15	153.41	192.85

Table 6: Temperature - Frequency

The unit for all the frequencies in this table is GHz (10^9 Hz).

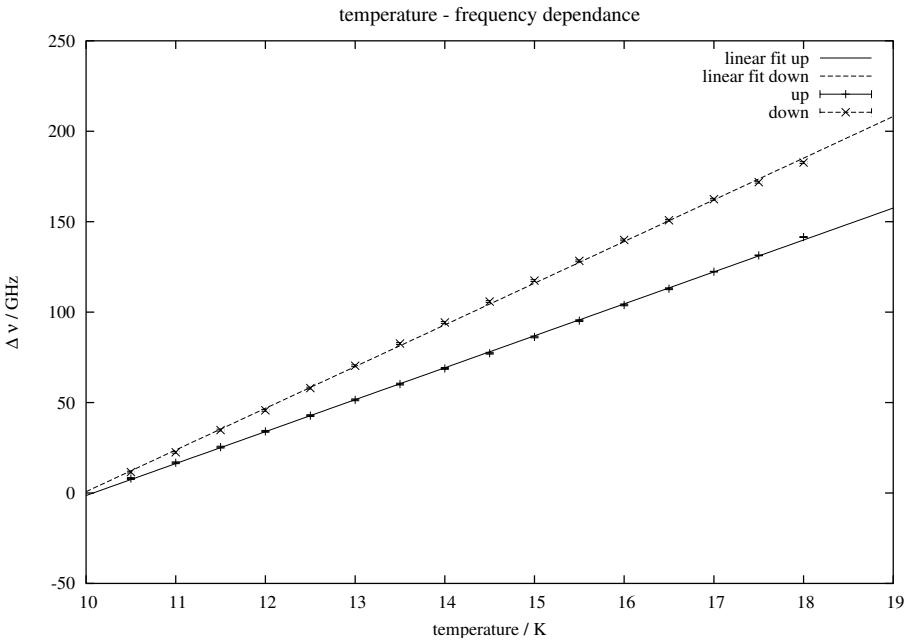

Figure 15: temperature-frequency (Fabry Perot)

results

The change of wavelength with an increase of the temperature by 1°K was in the measurement of the monochromator: $\Delta\lambda = 0.059 \pm 0.001$ nm for the rising temperature and 0.056 ± 0.001 nm for the decreasing temperature.
With the FP we measured $\Delta\nu = 17.66 \pm 0.07$ GHz upwards and 23.05 ± 0.14 GHz downwards.

2.6 current - frequency dependence

The principle of measurement is maintained, with the main difference, that now the temperature is fixed and the current is changed. We set the temperature to 17°C and increase the current in steps of 5 mA from from 50 mA to 115 mA. From there we decrease the current again in the same manner.

Monochromator		
I/mA	$\lambda_\uparrow$ /nm	$\lambda_\downarrow$ /nm
50	781.80	781.79
55	781.77	781.82
60	781.77	781.82
65	781.83	781.84
70	781.84	781.87
75	781.85	781.86
80	781.86	781.88
85	781.90	781.91
90	781.82	781.92
95	781.92	781.92
100	781.93	781.94
105	781.94	781.96
110	781.96	781.96
115	781.98	781.98

Table 7: Current - wavelength

Fabry-Perot-resonance			
I_{end} /mA	Δlines	$\Delta\nu$/GHz	$\sum\nu$/GHz
50			
55	6.5	9.43	9.43
60	6.3	9.14	18.56
65	6.3	9.14	27.70
70	6.2	8.99	36.69
75	6.3	9.14	45.82
80	6.1	8.85	54.67
85	6.2	8.99	63.67
90	6.0	8.70	72.36
95	6.0	8.70	81.06
100	6.0	8.70	89.76
105	6.2	8.99	98.75
110	6.2	8.99	107.74
115	6.3	9.14	116.87

Table 8: current - frequency

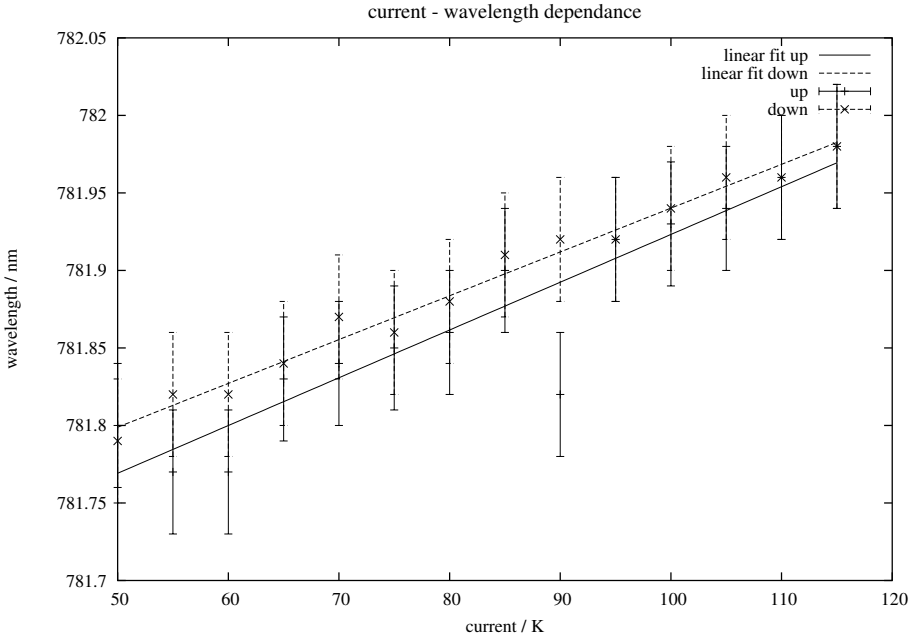

Figure 16: current-wavelength (Monochromator)

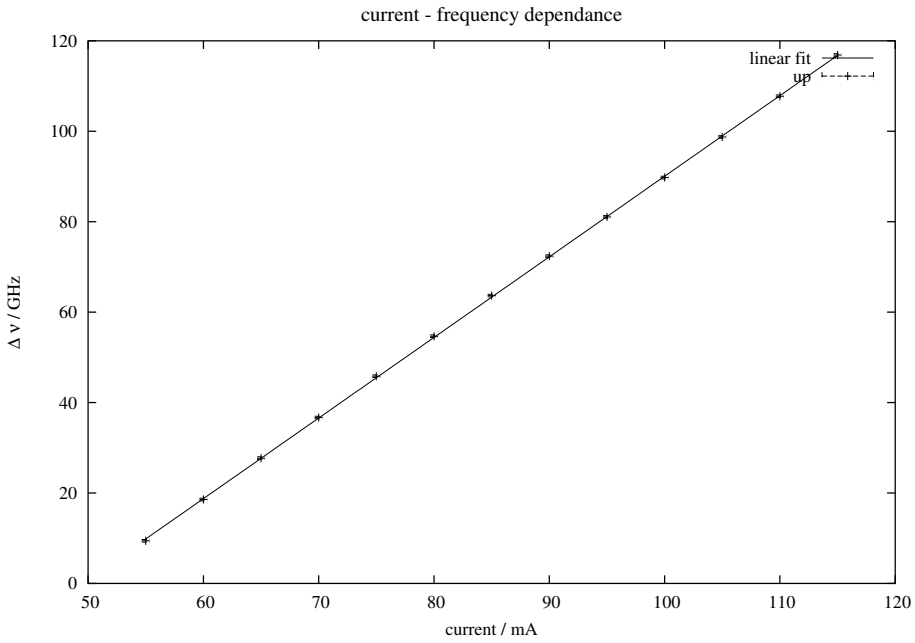

Figure 17: current-frequency (Fabry Perot)

results

The change of wavelength with an increase of the current by 1 mA was in the measurement of the monochromator: $\Delta\lambda = 0.0031 \pm 0.0004$ nm for the rising current and 0.0028 ± 0.0001 nm for the decreasing current.
With the FP we measured $\Delta\nu = 1.78 \pm 0.004$ GHz.

2.7 measurement of hyperfinestructure

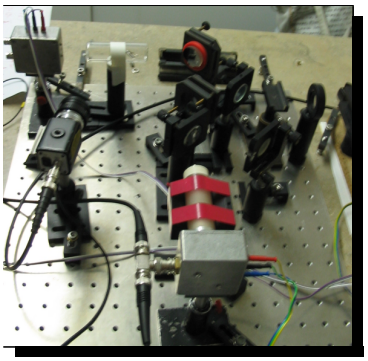

We insert the Rb glass tube in the beam and place a photodiode directly behind it. This can be seen in the picture of the setup. The CCD camera is used to observe the glass tube. Because of the very high background light from the environmental light we place a dark paper over the camera and Rb-tube to shield it from the background.

The resonance of th Rubidium can now be found (and seen) as fluorescence light on the screen and as drops on the oscilloscope because of absorption. After we had found the resonance we scanned the laser frequency with the sinus generator, so that we could see from the oscilloscope a small drop in the scan range. This picture has then been reproduced with a different (significant smaller scan frequency) on the x-y-writer. The paper of this is attached to the appendix.

calibration of grating monochromator

Without the frequency scan one can differ between four different fluorescence lines of Rb due to the hyperfine splitting. The center resonances of the Rb are at 780.24nm [from instruction papers], so we can use the grating monochromator to measure the frequency, and thereby calibrate the grating.

For the three separate resonances, we measure the frequency as 780.14nm, 780.16nm, 780.14nm, so the grating has a shift of approximately 0.1 nm from the correct value.

Rubidium hyperfinestructure

The calibration of th grating monochromator shows clearly that this device is not suitable for tiny and therefore precise frequency differences. Thus we record the frequency differences between the lines with the FP:

lines	FSR	$\Delta\nu$/GHz
1-2	2	2.90
2-3	2	2.90
3-4	1	1.45

We have to admit that this result is not very accurate, but the magnitude of difference in frequency between the lines is correct.

List of Tables

List of Figures

References

[Dem00] Demtröder. *Laserspektroskopie*. Springer Verlag, 4 edition, 2000.

[GPA93] Niloy K. Dutta Govind P. Agrawal. *Semiconductor Lasers*. Van Nsotrand Reinhold - New york, 2 edition, 1993.

[ILT] ILT. http://www.ilt.fhg.de/ger/optresonator.html.

[Mes99] Meschede. *Optik Licht und Laser*. Teubner Verlag, 1999.

[Sch02] Richard Scheps. *Laser Diode-Pumped Solid State Lasers*. SPIE Press, 2002.

[Sie86] Siegman. *Lasers*. University Science Books, 1986.